



Annual Review of Materials Research

Optical Metasurfaces: Progress and Applications

Shengyuan Chang, Xuexue Guo, and Xingjie Ni

Department of Electrical Engineering, The Pennsylvania State University, University Park, Pennsylvania 16802; email: xingjie@psu.edu

Annu. Rev. Mater. Res. 2018. 48:7.1–7.24

The *Annual Review of Materials Research* is online at matsci.annualreviews.org

<https://doi.org/10.1146/annurev-matsci-070616-124220>

Copyright © 2018 by Annual Reviews.
All rights reserved

Keywords

metasurfaces, 2D metamaterials, light control, phase control, resonant nanostructures, nanoantennas

Abstract

A metasurface is an artificial nanostructured interface that has subwavelength thickness and that manipulates light by spatially arranged meta-atoms—fundamental building blocks of the metasurface. Those meta-atoms, usually consisting of plasmonic or dielectric nanoantennas, can directly change light properties such as phase, amplitude, and polarization. As a derivative of three-dimensional (3D) metamaterials, metasurfaces have been emerging to tackle some of the critical challenges rooted in traditional metamaterials, such as high resistive loss from resonant plasmonic components and fabrication requirements for making 3D nanostructures. In the past few years, metasurfaces have achieved groundbreaking progress, providing unparallelled control of light, including constructing arbitrary wave fronts and realizing active and nonlinear optical effects. This article provides a systematic review of the current progress in and applications of optical metasurfaces, as well as an overview of metasurface building blocks based on plasmonic resonances, Mie resonance, and the Pancharatnam–Berry phase.

7.1



Review in Advance first posted on March 21, 2018. (Changes may still occur before final publication.)

1. INTRODUCTION

Scientists have long used the intrinsic properties of naturally occurring materials to build various optical components. Such components, for example, lenses, achieve wave front control through accumulated phase and amplitude change as light propagates inside the material. Therefore, those conventional optical components are constrained by the refractive index of the materials and the macroscopic structures of the components. The emerging 2D metamaterials (1), known as metasurfaces (2, 3), use an alternative approach for light manipulation based on abrupt and designable light modulation through subwavelength-thick elements. Those metasurfaces not only achieve the novel functionalities of their 3D counterparts, such as negative-angle refraction and invisibility cloaking, but also provide viable solutions to some of the limitations of 3D metamaterials, for example, high resistive loss and the complicated 3D fabrication process. Metasurfaces consist of subwavelength-sized meta-atoms, with spatially varying structural features or material compositions. They exhibit remarkable flexibility in manipulating the properties of light at an optically thin interface. Therefore, the high resistive loss accumulated in bulky 3D metamaterials is greatly mitigated with subwavelength-thick nanostructures. Moreover, metasurfaces are easy to fabricate using traditional nanofabrication techniques, including photolithography and electron-beam lithography, which are already commonly available in semiconductor industry.

Although the concept of a metasurface was proposed only a few years ago, artificially engineered structures have been widely adapted to control electromagnetic waves in multiple frequency regimes, for example, the frequency-selective surface (FSS) in microwave and blazed gratings as well as photonic crystals (4). However, metasurfaces differ from those structures in having spatially varying optical responses, which originate from localized interaction between light and meta-atoms, whose geometry and spatial distribution can be flexibly designed to generate desirable optical functions.

In this review, we systematically introduce the recent advances in metasurfaces and their major applications. We begin in Section 2 with a classification of metasurfaces regarding the material types of their constituents: plasmonic or dielectric. We explain the operating mechanisms of both designs. Sections 3–7 present some major applications of metasurface-based devices. In Sections 8–11, we discuss some unique physical properties of metasurfaces that were discovered in recent years; these properties give us a better understanding of the metasurface as a new platform for studying light-matter interactions. To conclude, we envision the future development of the metasurface technology.

2. META-ATOMS: BUILDING BLOCKS OF THE METASURFACE

Plasmonic materials, including metals and some transparent conducting oxides, transition metal nitrides, and 2D materials, display strong interaction with light through plasmonic resonances (5–8). In the process of interaction, electrons inside the material are shifted from their steady-state positions due to the external electrical field. Such behavior, known as polarization, generates an internal field to restore the electrons to their original places. Therefore, under a time-harmonic external field, a collective manner of oscillation is generated with a phase shift of π over the spectral width of the resonance. Moreover, depending on the size of plasmonic particles, they can be polarized either completely (for smaller particles) or only at the surface (for larger particles), resulting in a simple dipolar resonance or a multipole resonance. The resonant frequency of these resonances naturally depends on the shapes, materials, and surrounding media of these particles. Specifically, for larger particles, the effect of size and shape is more evident since the polarization happens mainly at the surface. Nevertheless, a 2π phase shift is required to provide full control of the wave front of the interacting wave. According to Huygens' principle (9), every point on a wave



front is a source of wavelets, which will spread out with the same speed as the source wave, and the line tangent to these wavelets forms the new wave front. On a plane metasurface, secondary waves reflected by or transmitted through the nanoantennas will gain different phase shifts, and thus they can interfere and generate an arbitrary wave front.

To increase the phase shift amount of single-mode dipolar resonance to 2π , researchers invented V-shaped nanoantennas (9, 10) that can support two resonant modes (**Figure 1a**): a symmetric mode and an antisymmetric mode. By superposition of those two resonance modes, a phase shift of 2π can be successfully achieved for the cross-polarized light, whose polarization is perpendicular to that of the incidence. Since there is a polarization conversion associated with the output light, the efficiency of this design is usually low. To overcome this limitation, researchers have adopted another design that incorporates a metallic ground plane separated from the top nanoantenna array by a thin dielectric spacer layer (11, 12). Light incident on this system will

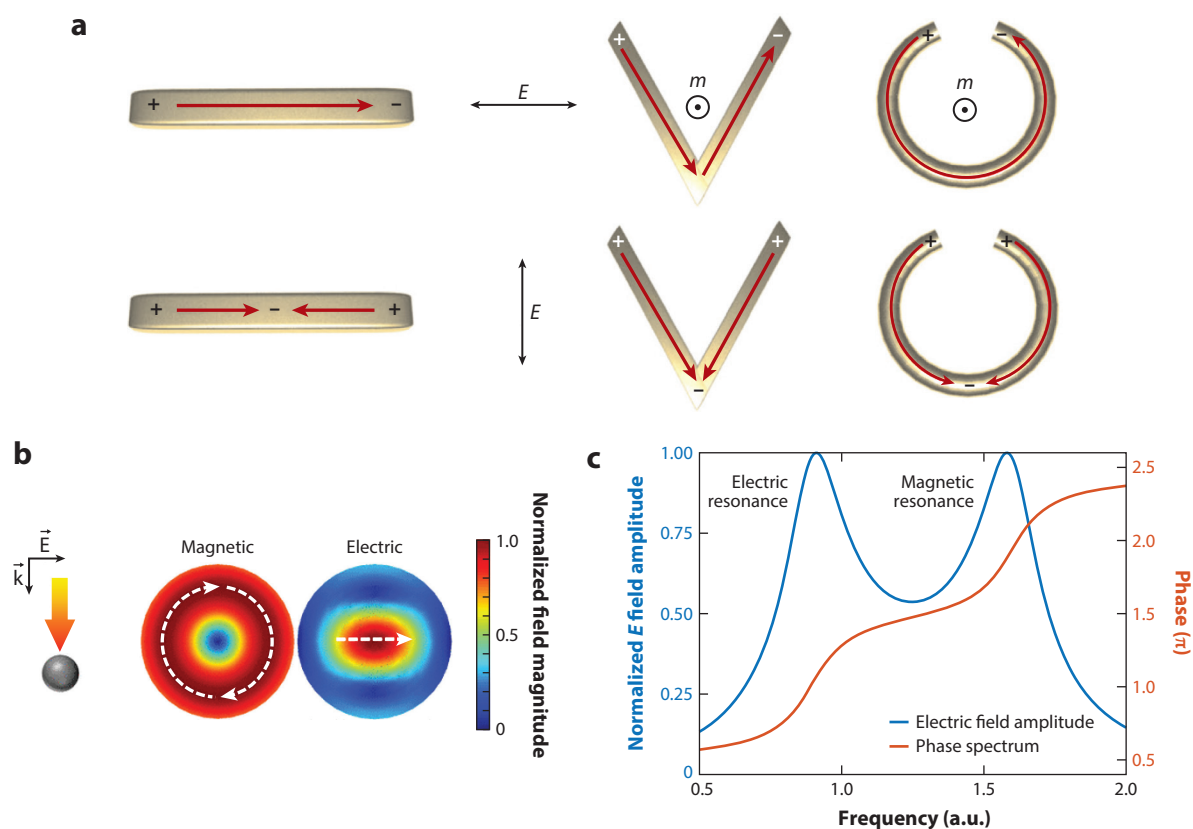


Figure 1

(a) Resonances in plasmonic nanoantennas. Different resonant modes are excited inside the antenna with different incident polarizations (denoted by E). Both electric modes (indicated by the red arrows) and magnetic modes (denoted by m) can induce a phase shift to the incident light. The shape and orientation of the nanoantenna [with respect to the electric field direction (denoted by E) of incident light] affect the excited resonances. (b) A sphere dielectric resonator is excited by a linearly polarized incidence (E denotes the electric field direction) at normal incidence (indicated by the wave vector k). The normalized electric field distribution is shown for a magnetic dipole and an electric dipole. The white arrows indicate the directions of the displacement current. (c) Illustration of the electric and magnetic dipolar resonances. When these resonances are perfectly overlapped, a phase shift of 2π can be generated. Panel *a* adapted with permission from Reference 5. Panel *b* adapted with permission from Reference 19.

induce antiparallel electric currents on the nanoantennas and the ground plane, creating a gap resonance and extending the phase shift to 2π . Furthermore, the hybridization of plasmonic resonance with the Pancharatnam-Berry (P-B) phase (13, 14) can also enlarge the phase shift range to 2π but works only for circularly polarized light.

Because plasmonic materials can provide strong optical resonances, they were chosen as the constituent materials of metasurfaces in the beginning stages of research (9, 10, 15), and many encouraging results were achieved. However, one of the most evident limitations of such plasmonic metasurfaces is that the energy of light tends to dissipate into heat in plasmonic materials (2). Similar problems also exist in phononic materials such as silicon carbide, in which the light-material coupling is carried out by the vibration of phonons instead of electrons (16). The resistive loss reduces the overall efficiency of the device, thus restricting them from many practical applications. Because plasmonic structures have great abilities in confining light in the nanoscale, incident light will quickly increase the local temperature. Therefore, plasmonic structures usually have a low input power threshold of deforming and/or destroying the nanostructures. In addition, noble metals, such as gold and silver, are widely used as the building materials for plasmonic structures, which increases the fabrication cost, and such use is incompatible with conventional semiconductor processes.

To break those limitations, novel designs of metasurfaces using purely dielectric materials were demonstrated (16, 17). Instead of coupling light to free electrons or phonons to create resonances, nanostructures made of dielectrics or semiconductors with high refractive indices, such as titanium dioxide, silicon, germanium, and tellurium, can manipulate the properties of light through Mie resonances (18) and can achieve enhancement for both the electric and magnetic fields. Since transparent dielectric materials usually have a small imaginary part of permittivity, only slight resistive loss is introduced to the structures by those materials. Such devices could maintain a substantially high efficiency. Moreover, making all-dielectric metasurface structures can be compatible with the current semiconductor processes.

A simple instance could be used to illustrate the resonance of dielectric nanoantennas. As shown in **Figure 1b**, for dielectric, sphere-shaped resonators, the two lowest resonant modes excited by the incident light are the electric and magnetic dipolar resonances (19). Higher-order modes are generally neglected, as they are orders of magnitude smaller in magnitude. The origin of the magnetic mode is similar to that of split-ring resonators, which results from the circulating displacement currents, leading to strong magnetic polarization in the center of the resonator. By overlapping the magnetic resonance with electric resonance, it is possible to achieve a phase change covering the entire 2π range (**Figure 1c**). Interestingly, when the electrical and magnetic dipole moments orient perpendicularly to each other, the scattered light is unidirectional, which can be readily realized in dielectric nanostructures to make reflection-free Huygens metasurfaces (20, 21). This behavior can be conceptually explained by the first Kerker condition, proposed in 1983 (22).

Aside from the plasmonic and dielectric metasurface designs based on dipolar resonances, researchers are also looking into coupled resonators exhibiting Fano resonances, which arise from the interference between a broad spectral line or continuum with a narrow discrete resonance (8, 23). With antennas with broken inversion symmetry, such as the asymmetric split-ring wire resonators, weak coupling of the plasmonic modes to free-space radiation modes can create narrow Fano-like resonances with narrow linewidth and high Q factor through interaction between a super-radiant broader dipole mode and subradiant magnetic dipoles (24). Fano resonances were also observed in pure dielectric systems (25–27) through coupling of magnetic and electric dipolar modes. The Fano resonance is directional (27) because the scattering wave is enhanced in one direction due to constructive interference and suppressed in the other due to destructive interference. The scattering direction is sensitive to frequency shift, which can be exploited in sensing

(28) and optical switching (29) applications. This type of resonance shows a new way to construct low-loss, nonlinear, and active metasurfaces (30).

In addition to resonance-based phase or amplitude modulation, there is also a different approach based on the P-B phase, namely the geometric phase, to achieve phase shifts. This method works only for circularly polarized light. In the early 2000s, Hasman and his coworkers (31–33) used space-variant subwavelength gratings to convert circularly polarized light into an arbitrary polarization or to form vortex beams. The building block of P-B phase metasurfaces can be viewed as wave plates with identical geometry but spatially varying orientations of fast axes. This space-variant polarization manipulation is easily explained by the Jones matrix (33):

$$\mathbf{T}(x, y) = \mathbf{R}(\theta(x, y))\mathbf{J}(\phi)\mathbf{R}^{-1}(\theta(x, y)),$$

where $\mathbf{J}(\phi)$ is the Jones matrix for a wave plate with retardation ϕ , \mathbf{R} is the rotation matrix, and θ is the local orientation of the fast axis of the wave plate. If right-handed $|R\rangle$ and left-handed $|L\rangle$ circular polarized (RCP and LCP, respectively) light is incident on the metasurface, the resulting light beams will have the following form:

$$\begin{aligned} \mathbf{E}_{\text{output,RCP}} &= \mathbf{T}(x, y)|R\rangle = [\cos(\phi/2) - i \sin(\phi/2) \exp(-i2\theta)]|L\rangle, \\ \mathbf{E}_{\text{output,LCP}} &= \mathbf{T}(x, y)|L\rangle = [\cos(\phi/2) - i \sin(\phi/2) \exp(i2\theta)]|R\rangle. \end{aligned}$$

It is evident that a RCP or LCP light will be converted into the opposite circular polarization and will lose or gain an additional spatially variant phase $2\theta(x, y)$, respectively. If the unit cell of the wave plate is rotated from 0° to 180° , the induced phase shift can be continuously tuned from 0 to 2π . The phase shift is purely geometric and independent of any dispersive resonances, and therefore it has a broad operational bandwidth. Its performance is limited only by nanoantenna scattering efficiency. In contrast, P-B elements can be resonantly excited to increase the scattering efficiency, but the phase shift still mostly comes from the geometric phase.

So far, we have addressed an overall mechanism of the building blocks of metasurfaces. Below, various metasurface-based applications are introduced to cover the topics of current metasurface research.

3. METASURFACES FOR LIGHT BENDING AND FOCUSING

Metasurfaces can introduce abrupt phase changes at the interface, which originates from the various mechanisms mentioned in Section 2. Relative to conventional optics, where phase is accumulated along the propagation path of light, metasurfaces provide a simpler solution to engineer phase directly within an optically thin layer.

3.1. Phase-Gradient Metasurfaces

With that phase engineering capability, we can artificially introduce a linear phase gradient on a surface. Similar to the fact that the behavior of light at the interface of two media is governed by the traditional Snell's law of reflection and refraction, light behavior at a phase-gradient metasurface can be described by the generalized Snell's law. It can be derived utilizing Fermat's principle of light propagation, which indicates that light must travel along a path with minimal propagation time. Yu et al. (9) were the first to propose and demonstrate the generalized Snell's law. **Figure 2a** vividly illustrates (3) the generalized Snell's law and its difference from the classical one. This illustration mimicked Feynman's example (3, 34) of a coast guard saving a drowning man, which was used to represent the classical Snell's law. Since the swimming speed and the running speed of the guard are not the same, the path that takes the shortest time is not a straight line connecting the start and the destination but is instead a polyline, which bends at the interface between two

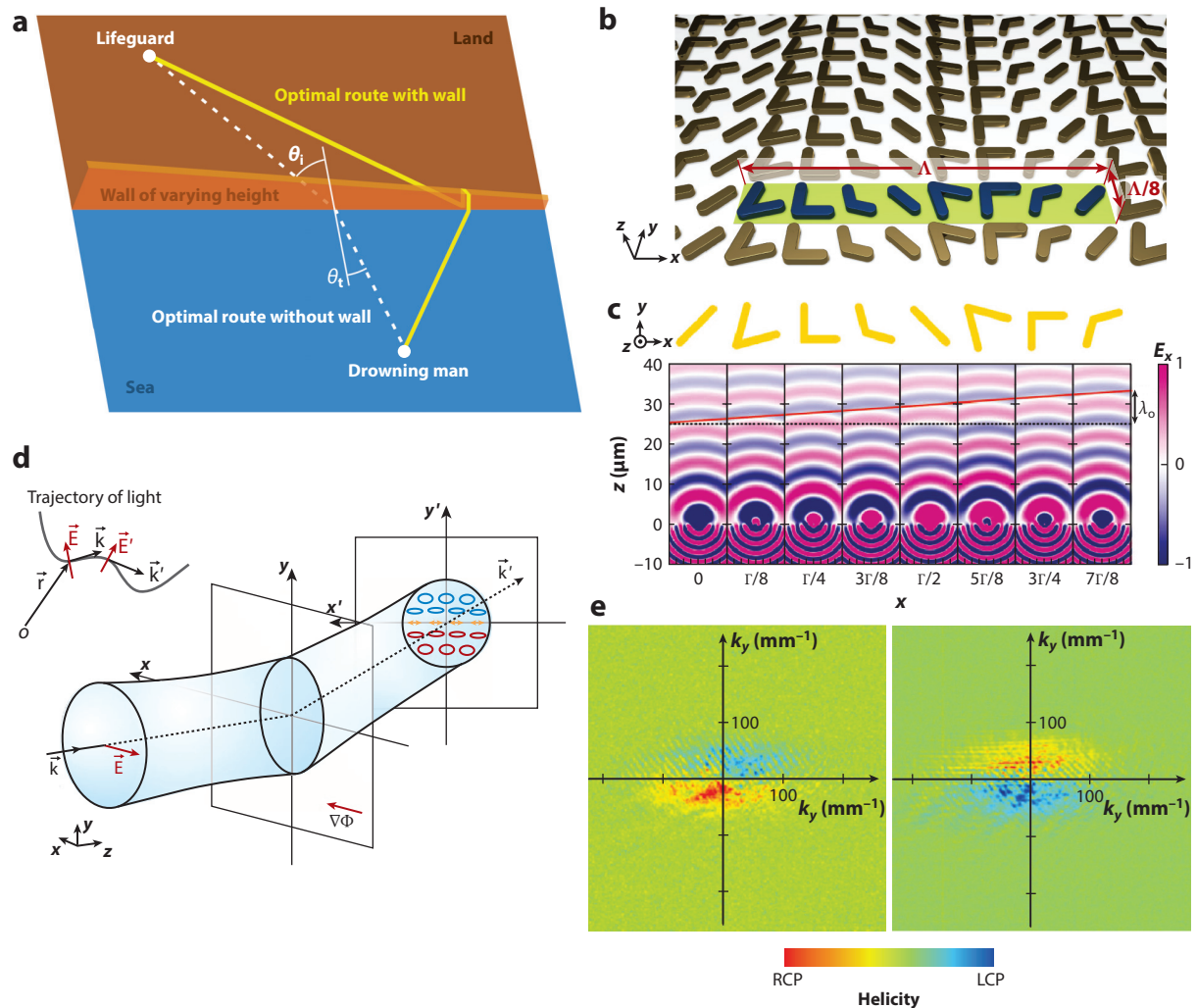


Figure 2

Phase-gradient metasurfaces. (a) The drowning-man example of the refraction of light at the interface between two media. (b,c) Schematic view and phase profile of V-shaped plasmonic nanoantennas. (b) A supercell consisting of eight nanoantennas, with a length of Λ and a width of $\Lambda/8$. (c) A design similar to that of panel b is shown, and the length of the supercell is denoted by Γ . The wave front of the scattered light has a propagation distance difference of a free-space light wavelength λ_0 across a supercell, corresponding to a phase difference of 2π across the eight nanoantennas. A phase gradient causing the transmitted light to bend is observed. (d) Conceptual image of a metasurface-enhanced photonic spin Hall effect (PSHE) measurement. In the image, the electric field direction (polarization) is indicated by \mathbf{E} , and the propagation direction of light is denoted by \mathbf{k} . The metasurface generates a phase gradient ($\nabla\Phi$) that bends the transmitted light and causes the splitting between the right circular polarization (RCP) and the left circular polarization (LCP), indicated by the red and blue circles, respectively. The spin-orbit interaction, which originates from the transverse nature of light, is depicted at the upper left corner. This phenomenon is considered to be the origin of PSHE. (e) Incident light that is x -polarized and y -polarized will have different PSHE after refraction on the metasurface plane. Adapted from Reference 3 (panel a), Reference 10 (panel b), Reference 9 (panel c), and Reference 41 (panels d and e), with permission.

different media. By introducing a metasurface, however, a wall of spatially varying height is added. If we suppose that the time taken for the guard to climb up the wall is proportional to the wall's height, the path of the guard varies again since he must take into consideration the time to climb the wall. Following a simple mathematical calculation, we may find the optimal path, which coincides with the prediction from the generalized Snell's law.

The generalized Snell's law was first verified experimentally using V-shaped plasmonic nanoantenna arrays (9, 10) in the mid-infrared and near-infrared range (**Figure 2b,c**). As we discuss in Section 2, two plasmonic eigenmodes are supported in V-shaped antennas. By utilizing the superposition of these eigenmodes, a phase change varying from 0 to 2π (**Figure 2c**) can be added to the cross-polarized component of the scattered wave. The value of this additional phase can be controlled by the dimensions and orientation of those nanoantennas. Moreover, the amplitude of the y -axis polarized component should be kept constant to maintain a uniform wave front. By sampling the additional phase with a $\pi/4$ increment and arranging the nanoantennas with corresponding phase in one direction, the phase gradient is formed at the metasurface plane, which was used to demonstrate the generalized Snell's law.

Later demonstrations using reflection-mode metasurfaces (11, 12) were also reported. In those configurations, nanoantennas are used to introduce a phase gradient on the metasurface plane, and a metallic ground plate is placed underneath. A dielectric spacer layer is sandwiched between the nanoantenna layer and the ground plate. Due to the presence of the metallic ground plate, the nanoantennas could couple with their images to double the range of the phase shift, which makes it easier to cover the full 2π phase range. Additionally, the metasurface in reflection mode will significantly improve the reflectance efficiency since the transmission is eliminated by the ground plate, and the polarization state of the reflected wave will remain the same as that of the incident wave.

3.2. Photonic Spin Hall Effect

The spin Hall effect (SHE) (35) refers to the phenomenon in which electrons with opposite spin gather at opposite lateral surfaces of a conducting medium carrying electric current. Such an effect originates from the spin-orbit coupling of electrons and results in the development of spintronics. Photons, as the basic unit of light, also have similar spin-orbit interaction in the medium it propagates, and hence the photonic analog of SHE—the photonic SHE (PSHE) (36, 37)—can be introduced with inhomogeneity of the refractive index of the medium. Light will be refracted when traveling in such a medium. The refraction will generate a geometrical phase, which lead to a lateral split between two opposite circular polarizations. This effect is termed the PSHE.

The experimental observation of such a PSHE phenomenon is a challenging task since the momentum carried by the photon and its spin-orbit interaction with the medium is very small relative to electrons. In previous attempts, multiple reflections or quantum weak measurements (38) were used to observe the PSHE. However, these methods require an extremely precise experimental setup. In addition, one of the premises of the PSHE, the conservation of total angular momentum at anywhere on the beam (39), might break since the measurement employs some wavelength-scale structures.

Recent research (40, 41) reported that a metasurface can gigantically enhance the photonic spin-orbit interaction by inducing a rapidly varying phase gradient to destroy the axial symmetry of the optical system (**Figure 2d**). Such a phase gradient should be aligned with the polarization direction of a linearly polarized incident light, and two circularly polarized components (LCP and RCP) can be observed to accumulate at the opposite lateral directions (**Figure 2e**). In an experimental setup to observe metasurface-enhanced PSHE (41), arrays of V-shaped phase-shifting nanoantennas were used to generate phase gradients, which were used to bend light with a large angle. Since

the refraction happens within an ultrathin layer, a large geometrical phase was introduced, and therefore a large PSHE was observed. As the experiment suggests, metasurfaces could be used to provide controlled inhomogeneity at the interface, which could offer a reliable way to utilize the spin degree of freedom of light.

3.3. Metalenses

It is possible to create metasurface-based flat lenses, i.e., metalenses, with the same functionality as traditional lenses exploiting phase control capability. Metalenses are created by forming a parabolic phase profile provided by spatially arranged phase-shifting nanoantennas. Earlier designs of metalenses involved V-shaped nanoantennas or nanovoids (42), which are considered equivalent in the perspective of optical scattering, as shown in the simulation results presented in **Figure 3a**. Since the metalenses do not rely on polished spherical surfaces, they do not suffer from spherical aberrations by nature (43). However, the fixed subwavelength pattern of metalenses resulted in evident

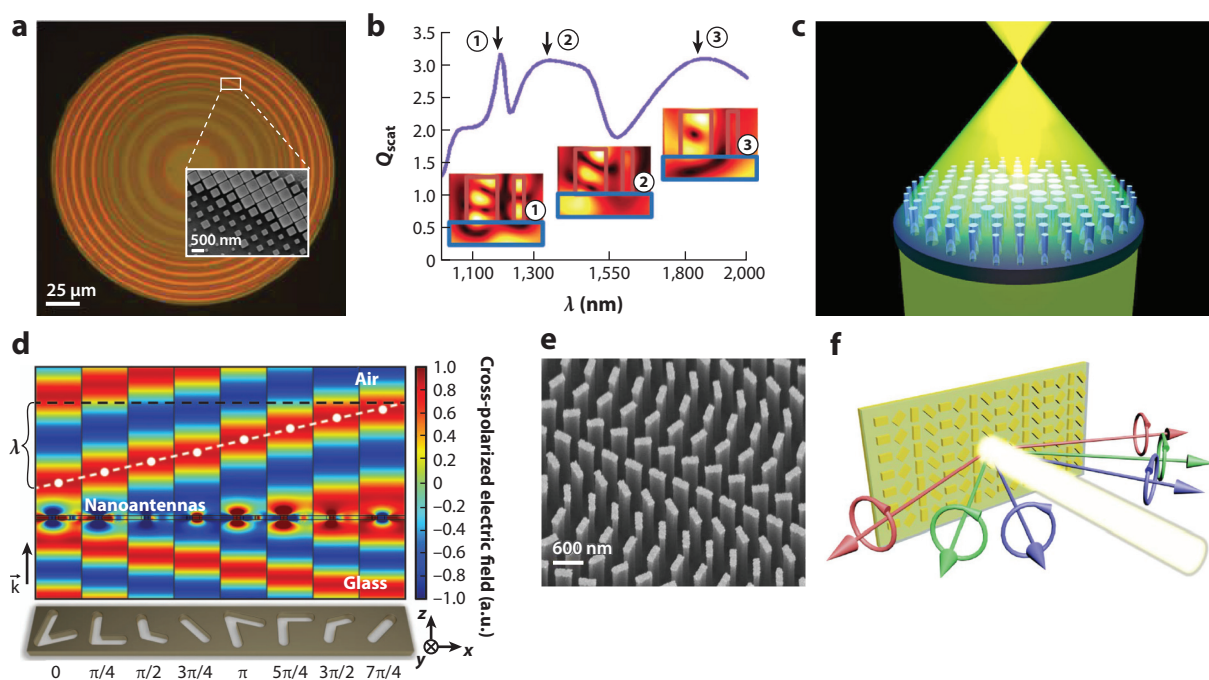


Figure 3

Metalenses. (a) Design of an achromatic metalens and its SEM images (*inset*). (b) Scattering efficiency (Q_{scat}) of paired nanoantennas changing with wavelength. In each unit cell of the metasurface, two antennas are placed together. The two coupled nanoantennas could achieve high-efficiency scattering at three wavelengths (labeled as ①, ②, and ③), where achromatic metasurfaces are designed. The distributions of the electric field for each labeled point are depicted. (c) Conceptual image of a polarization-insensitive metasurface. Highly symmetric structures are used to reduce the polarization sensitivity. (d) Full wave simulation of the wave front generated by a V-shaped nanovoid array. These nanovoids serve as nanoantennas following Babinet's principle. The light is incident from the glass substrate side, the direction of which is denoted by the wave vector \mathbf{k} . (e) An SEM image of a superdispersive metalens for high-resolution spectroscopy. Nanoantennas are placed with spatially varying orientations for generating phase gradient. (f) Conceptual image of an on-chip chiroptical spectrometer using a metasurface. By utilizing the photonic spin Hall effect of metasurfaces, this device splits light with opposite spin and different wavelengths (denoted by the differently colored arrows). Adapted from Reference 45 (panel a), Reference 44 (panel b), Reference 46 (panel c), Reference 42 (panel d), Reference 49 (panel e), and Reference 50 (panel f), with permission.

chromatic aberrations (44, 45), which became a major challenge for researchers. To overcome this issue, designs of achromatic metalenses (**Figure 3a**) were recently discussed. One method to reduce chromatic aberrations is utilizing dispersive phase compensation. In a recent work from Aieta et al. (44), such compensation is accomplished using a specially designed metasurface, whose constituent meta-atoms consist of two coupled dielectric nanoantennas of rectangular shape, as shown in **Figure 3b**. The coupling between these two antennas results in high-efficiency scattering at three different wavelengths, and the subwavelength array of such antenna sets generates phase changes to focus light. In this way, the chromatic aberration is eliminated at three wavelengths.

Another task is to eliminate the polarization dependence of the metalenses. Such dependence is attributed to the nonsymmetrical shape of optical nanoantennas and subwavelength patterns and could be reduced or eliminated by using highly symmetric shapes. A polarization-insensitive design of a metalens (46) was recently presented using transition-metal oxide nanopillar antennas. **Figure 3c** shows an illustration of that metalens. To achieve higher symmetry, the meta-atoms of the metasurface are of cylindrical shape and are arranged in a circularly symmetric fashion.

Metalenses have shown great flexibility in light focusing and imaging, and such flexibility originated in digitized designs of the subwavelength-scale patterns. By designing and optimizing these patterns, we could improve the performance of metalenses to achieve higher efficiency (47), higher numerical aperture (48), and a broader range of working wavelengths. One typical design of metalenses that was recently proposed (49) showed transmissive metalenses with high spectral resolution and compact size for near-infrared light. In particular, large-angle off-axis focusing was achieved with the metasurface, of which an SEM image is shown in **Figure 3e**. This work shows that metalenses could overcome the challenge of designing high-resolution off-axis lenses.

The functionality and compactness of the metalens make it an ideal alternative to conventional lenses, especially in cases in which the space of optical systems is limited. A successful practice utilizing metalenses in compact systems is the on-chip chiral spectrometer (50), whose conceptual image is shown in **Figure 3f**. In this setup, two kinds of metasurface-based devices are used. One is the meta-grating, which splits light with different wavelengths. The other is a metalens used to focus these split lights to different positions of the image plane, where a CMOS camera is placed to measure the intensity of the focused light. Such a device achieved spectral resolution as low as 0.3 nm, and such resolution is limited by the CMOS detector. A working wavelength range of 170 nm was also achieved. Moreover, metalenses could also be used in imaging systems, with a broad wavelength range from visible light to microwave. A recent publication of a typical imaging system utilizing a metalens (51) presented an immersive metalens for microscopy. The metalens was integrated with a commercial scanning confocal microscope to achieve a spatial resolution as low as 200 nm and a high numerical aperture of 1.1. In conclusion, some conventional lenses could potentially be replaced by metalenses, thus shrinking the system size and sometimes also improving performance. For instance, Groever et al. (52) designed a metalens doublet by fabricating metalenses on both sides of a dielectric substrate, which is analogous to the doublet lenses in classical optical systems. By combining the compactness of the metalenses and the aberration-correction capability of the classical optical systems, we are moving one step further to the mass production of high-end metalenses.

4. METASURFACES FOR POLARIZATION AND ANGULAR MOMENTUM CONTROL

4.1. Polarization Conversion

Polarization, as a physical property and a degree of freedom of light, has great significance in almost all kinds of optical systems. Effective methods to control polarization states, as a result,

have been highly emphasized in past research in optics and photonics. Metasurfaces, with the promising capability of phase engineering with ultralow thickness, can result in the extraordinary manipulation of polarization states by designing specific patterns of nanoantennas.

Wave plates are widely used in a vast variety of optical systems. These optical components could shift the polarization state of polarized light by introducing certain phase differences to two orthogonal components of light (53). Similar to the working mechanism of conventional wave plates, metasurfaces realize polarization conversion through manipulation of two eigenmodes of light that correspond to two orthogonal polarizations (54). To design a metasurface for polarization conversion, one should have knowledge of the incident wave and the desired output wave. With such information, a Jones matrix at each point on the metasurface plane, which connects the incident and output waves, can be calculated. The calculated Jones matrix can be achieved by designing the proper meta-atoms.

One of the earliest works on polarization control with metasurfaces utilized plasmonic V-shaped antennas (55). In this work, researchers converted incident linearly polarized light to circularly polarized light. Such conversion is performed through superposition of two scattering light waves with approximately the same amplitude, orthogonal linear polarizations, and a $\pi/2$ phase difference. The V-shaped antennas are divided into two sets to generate two types of scattering light, with a $\pi/4$ angular difference between the orientations of corresponding antennas in different groups.

Up to now, the conversion between a linear polarization state and a circular polarization state, between two different linear polarization states, or between two opposite circular polarization states (i.e., between RCP and LCP states) has been reported with experiments using metasurfaces (54, 56, 57). One way to achieve such conversions by a metasurface—a combination of a propagation phase and a geometrical phase—was implemented using spatially varying patterns of nanoantennas. The geometrical phase (32, 33, 54, 56, 58), as we introduce above, could be generated by composing the metasurface with identical nanoantennas with spatially varying orientations, as shown in **Figure 4b**. However, since one major limitation of P-B phase-based metasurfaces is that they work only for circularly polarized incident light, the P-B phase itself must be combined with the propagation phase to achieve arbitrary control of polarization states, which leads to a hybrid pattern of nanoantennas (**Figure 4a**).

4.2. Spin-to-Orbit Angular Momentum Conversion and Orbital Angular Momentum Generation

Polarization-controlling metasurfaces combining the propagation phase and the geometrical phase could also be used in the generation of optical vortex beams, which are also termed orbital angular momentum (OAM) beams since they carry OAM (59, 60). The most significant feature of such OAM beams is their helix-shaped wave front, which is a direct consequence of its phase dependence on azimuthal angle. The order of OAM, L , is described as the number of the twists of a wave front contained per unit wavelength. OAM has been recognized as an additional degree of freedom of light (59) and could be utilized in high-speed free-space optical communication systems (61, 62) since beams with different orders of OAM will not interfere with each other.

Traditional methods of OAM beam generation include the use of laser-mode conversion (60), spatial light modulators, and other optical devices such as spiral phase plates (63). Metasurfaces, however, can directly create a helical wave front for the output beam by arranging nanoantennas with linearly increasing (or decreasing) phase shifts along the azimuthal direction (9). Thus, such metasurfaces add an optical vortex to the light wave front, which is shown in **Figure 4c**. This kind of spatial arrangement for the phase shifts can be done for circularly polarized light as well as for exploiting the P-B phase. Since, as a result, this arrangement turns spin angular momentum

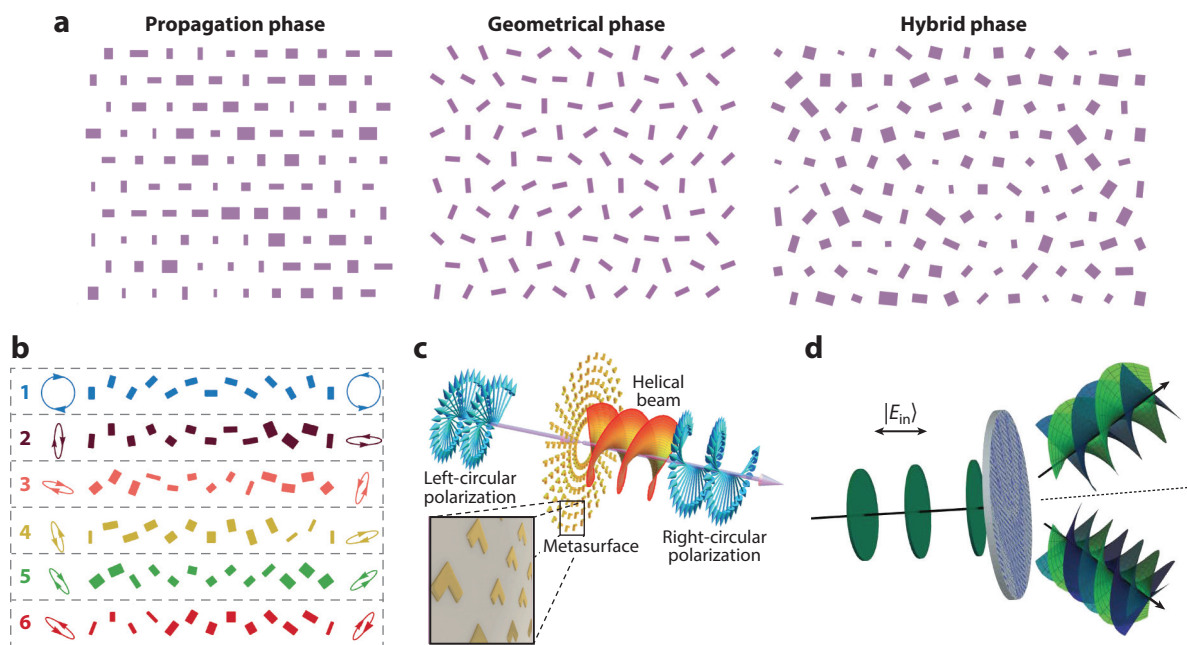


Figure 4

(a) Illustration of metasurface nanoantenna arrays generating the propagation phase, the geometrical phase, and the hybrid phase. (b) Six sets of nanoantennas (numbered 1 through 6) for splitting different orthogonal polarization states of light. These six sets of nanoantennas could deflect the corresponding orthogonal polarization states to opposite directions with respect to the surface normal. Since the first set uses only the geometrical phase, it can split only circularly polarized light. For sets 2–5, the propagation phase is combined by changing the dimensions of the nanoantennas, enabling them to split elliptically polarized light with different polarization orientations. (c) Spin-to-orbit conversion (SOC) using a metasurface. This device reverses the spinning of incident light and attaches an additional type of angular momentum—orbital angular momentum (OAM)—to the output light. (d) SOC-based OAM generation and splitting with incident light, whose wave fronts are shown as dark green, of an arbitrary polarization state $|E_{in}\rangle$. The helical wave fronts of two output light beams are shown on the right in light green and dark blue. Adapted from Reference 54 (panels a and b), Reference 65 (panel c), and Reference 64 (panel d), with permission.

(carried by the circularly polarized light) to OAM, it is also termed spin-to-orbit conversion (SOC) (64, 65). Normally the SOC permits only the conversion of left- and right-circular polarizations into states with opposite OAM. However, by providing an additional phase shift in the azimuthal direction, a metasurface can convert circular polarizations into states with independent values of OAM, as shown in **Figure 4d** (64).

5. METASURFACE INVISIBLE CLOAKS

An invisibility cloak is an optical device used to conceal an object and to render it invisible. It was scientifically realized thanks to transformation optics and conformal mapping. However, the initial proposal for an invisibility cloak involved extreme values of material properties, which are hard to achieve practically. Later, a so-called carpet cloak circumvented this issue by transforming a bumping, reflecting surface into a flat one. This technique, which is termed quasi-conformal mapping (66), has been used in both the microwave and optical regimes to create cloaking devices. The idea of quasi-conformal mapping frees researchers from the endless seeking of certain materials with desirable refractive indices, but practically there are still some major limitations

for current cloaking devices that employ such a technique. For example, the reshaping of the wave front requires a spatially varying refractive index, which usually takes a large volume of the cloaking device, making it bulky and hard to scale up to a macroscopic scale. Moreover, light propagation inside such material regions also causes additional phase retardation, which makes the cloaked object detectable by phase-contrast devices.

Unlike traditional cloaking devices, a metasurface cloak directly reshapes the wave front of the reflected light by compensating for the phase difference at different locations on the cloaked surface. The phase shifts needed are provided by the nanoantennas, which are arranged with subwavelength spacing. Such compensation could be maintained within a certain range of incident angle. Therefore, the metasurface cloak (67–69) renders the object underneath invisible. Ni et al. (67) recently realized such a metasurface-based cloak by using rectangular gold nanoantennas, which were fabricated on a 3D curved surface, as illustrated in **Figure 5a**. The arbitrarily shaped

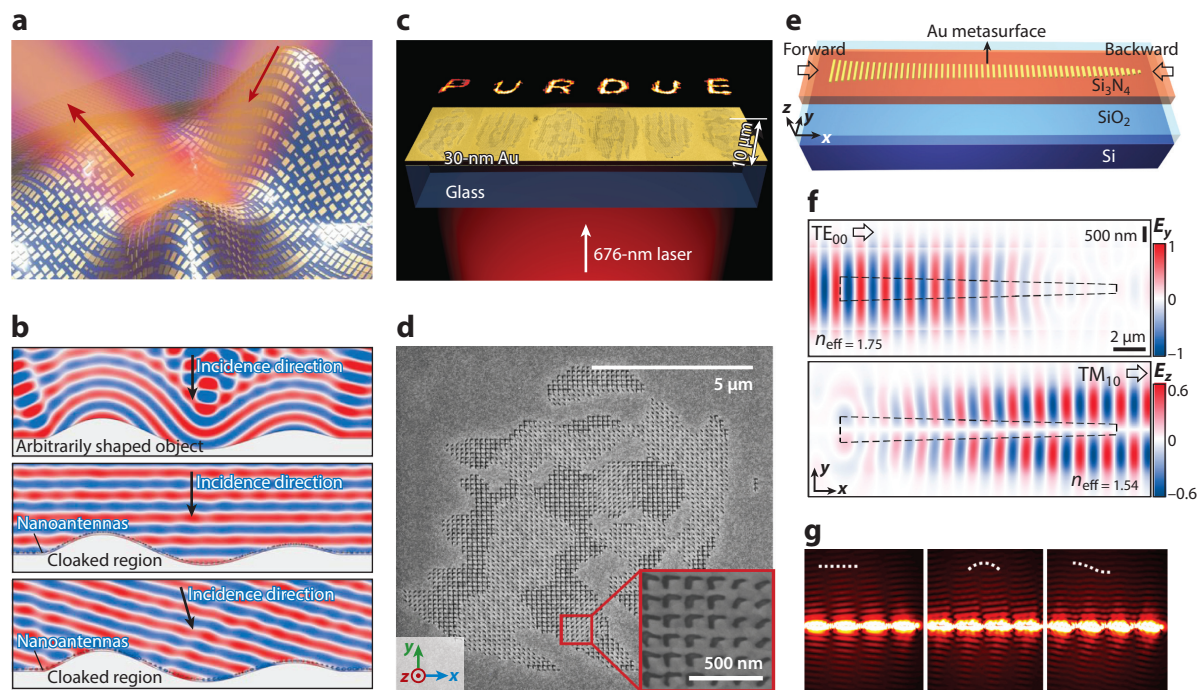


Figure 5

(a) Conceptual image of a metasurface optical cloak. The red arrows indicate the directions of the incident and reflected light. The gold nanoantennas of the metasurface cloak are depicted as shiny rectangular blocks on the curved surface. (b) Reflected fields for a surface without and with a metasurface cloak. Oblique incidence is also considered for the cloaked condition. The colors indicate the wave fronts of the reflected light. (c) A metasurface hologram with the generated holographic image “PURDUE” when illuminated by a 676-nm laser. (d) An SEM image of the metasurface hologram for the letter P. The inset at bottom right shows the V-shaped nanoantennas that are the building blocks of the metasurface hologram. (e) Schematics of a 1D metasurface for mode coupling and conversion. Light incident from different sides will be coupled differently. (f) Coupling between TE (transverse electric), TM (transverse magnetic), and surface waves. Here, TE (TM) waves are defined as waves that have a nonvanishing electric (magnetic) field component along the propagation direction, and they have distinguishable effective modal indices (n_{eff}). The TE_{00} mode can be coupled to the TM_{10} mode if incident from the left side (forward) while coupled to surface waves if incident from the right side (backward). The coupling between these modes can be seen from the amplitude distribution of the electric field (E_y denotes the y component and E_z denotes the z component of the electric field). (g) Simulation images of metasurface-generated surface waves with various wave fronts (denoted by the white dots). The intensity distributions of the electric field are shown to depict the wave fronts of the excited surface waves. Adapted from Reference 67 (panels a and b), Reference 73 (panels c and d), Reference 74 (panels e and f), and Reference 78 (panel g), with permission.

3D object is perfectly concealed, with only a plane wave reflection observed, as the simulation shows in **Figure 5b**.

6. METASURFACE HOLOGRAMS

The emerging trend of virtual reality and augmented reality has led to a greater demand for effective methods for 3D display than ever before. Holography, an optical approach to record and restore 3D images, is therefore of tremendous interest. The traditional holography technique (53) requires the interference of a coherent reference beam with the object beam to generate an amplitude hologram, which can reproduce the 3D image of the object if a readout beam is applied to it. However, such a hologram suffers from low image brightness since a conjugate image is produced along with the real image during the readout process. Later on, phase holograms were proposed as an improvement (70), which translates the interference pattern during the recording process to phase distribution while setting the amplitude on the hologram plane to be uniform. Such phase holograms could significantly improve the brightness of the recovered image, but the conjugate image still exists.

With the rapid development of nanofabrication techniques, this limitation could be overcome by employing metasurface holograms. Since metasurfaces could manipulate the phase distribution at the hologram plane at a subwavelength scale, the conjugate image could be eliminated (71, 72). An example of a metasurface hologram (73) appears in **Figure 5c**, which shows the fabricated metasurface on the hologram plane. Spatially distributed nanoantennas (**Figure 5d**) were used to provide phase and amplitude information when read out, so that the original scattering wave from the object can be reconstructed and its holographic image revealed.

The general process of metasurface-based holography is similar with computer-generated holography techniques: First, the object wave is calculated at the hologram plane. Second, the nanoantennas of the metasurface are designed to provide phase shift and amplitude modulation to the output wave. Such phase shift should have a coverage of 2π to cover all possible phase values. Finally, the phase and amplitude of the object wave at different points on the hologram plane are sampled, and nanoantennas with corresponding phase and amplitude modulation are placed at these points.

7. METASURFACES FOR SURFACE OR GUIDED WAVES

With carefully designed subwavelength arrays of nanoantennas, metasurfaces form abrupt phase changes on their surfaces. Such spatially varying phase changes could be regarded as an additional wave vector, which serves as compensating momentum between different propagating modes, thus enabling metasurface-based wave coupling. Since the coupling between modes inside an optical waveguide is extremely important in optical communication systems such as optical fibers, the effects and properties of metasurfaces in wave guiding and coupling are well worth investigation.

7.1. Mode Conversion

Metasurfaces allow for complete control of the flow of light, which provides unforeseen utility in integrated optics. Recent research (74) proposes a 1D metasurface-embedded waveguide structure for mode coupling and conversion, as shown in **Figure 5e**. Since the metasurfaces introduce a phase gradient on the waveguide top surface, an equivalent wave vector \mathbf{k} is applied along the waveguide, which provides an additional wave vector for mode coupling and conversion to happen. With the directionality of such a wave vector, such mode conversion is also directional (as seen in **Figure 5f**).

7.2. Surface Wave Control

Metasurface can also be designed for surface-wave manipulation. Surface plasmon polaritons (SPPs) can exist at a metal-dielectric interface, with large propagation wave vectors and tight field confinement. By using metasurfaces as a coupler, the momentum difference between the free-space incident wave and the SPPs can be compensated for by the phase gradient, which can be considered as an equivalently linear momentum provided by the metasurface. Unlike the conventional grating couplers, the momentum provided by the metasurface points to a unique direction, and therefore the SPPs and their low-frequency counterparts (i.e., spoof SPPs on artificial surfaces) can be excited unidirectionally (11, 75–77). Anisotropic SPPs propagating in one direction were recently reported using metasurfaces consisting of V-shaped bimodal nanoantennas as a coupler (78). As we discuss above, such antennas could support two orthogonal electrical dipole modes (16), which could be used to generate asymmetric SPP wave fronts, as observed in **Figure 5g**. This induced SPP could also be combined with other modes supported by the metasurface, providing more possibility for exotic optical properties.

8. METASURFACES FOR REMOTE QUANTUM INTERFERENCE

In ordinary isotropic quantum vacuum, the quantum interference is unlikely to happen, since it requires nonorthogonal transition dipole moments, which can hardly be seen in different excited states of an atomic system. However, in anisotropic quantum vacuum (AQV), quantum interference can be achieved even with orthogonal transitions. Current research has predicted that AQV could be generated by embedding an atom in a photonic crystal or near a metallic plane, but realizing either possibility requires extraordinarily precise positioning (79, 80) of the atom. In addition, in such a short distance between the atom and the surface, the property of the atom can be greatly affected by short-range effects such as the Casimir-Polder force and surface thermal noises. Hence, observing quantum interference in practical systems is very difficult with these methods.

Metasurfaces, with the capability of direct phase engineering in a polarization-dependent way, provide us with another route to generating AQV. A recent work (81) proposed and theoretically demonstrated AQV generation with a metasurface. In this approach, as shown in **Figure 6a**, two orthogonal dipole moments parallel to the metasurface from an atomic system can be reflected in different ways: One focuses to itself, and the other defocuses, allowing for quantum interference between the two dipolar modes.

This behavior can be achieved by designing a set of nanoantennas to have a constant phase shift in one polarization and a linear phase shift in its orthogonal polarization, as shown in **Figure 6b**. If those nanoantennas are arranged such that the latter polarization forms a parabolic phase profile, as shown in **Figure 6c**, the incident light with that polarization will focus as if it were reflected by a spherical mirror, while the other polarization will experience a flat mirror. Therefore, if the isotropy of the quantum vacuum in the focusing point (the center of the spherical mirror) is broken, these orthogonal photons generated at that point can have quantum interference with each other.

From the calculations in Reference 81, generated AQV could be maintained within a distance as far as 100 wavelengths, which is considered a macroscopic distance compared to the distance achieved by previous methods. This research demonstrates the capability of metasurfaces in quantum optics systems, and this new AQV generation technique could be applied in quantum communication and quantum computing systems.

9. NONLINEAR METASURFACES

The nonlinearities in optics have long been studied and utilized to manufacture optical devices. In recent years, there has been a growing tendency to incorporate nonlinear phenomena and



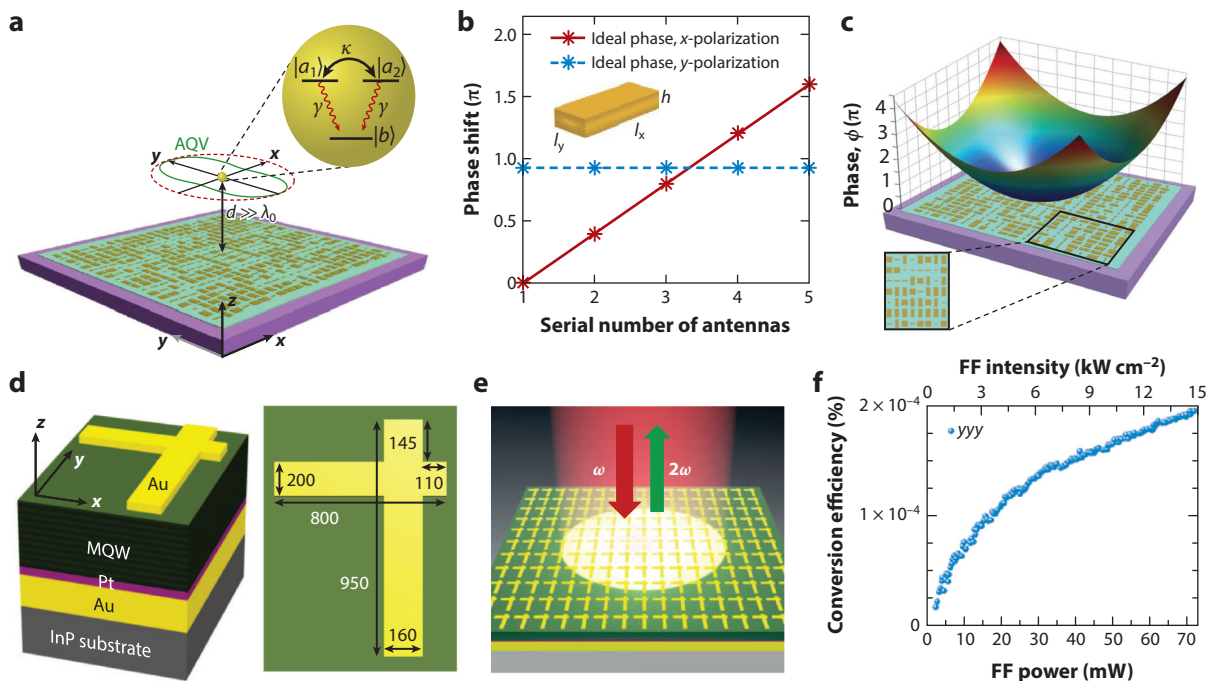


Figure 6

(a) Anisotropic quantum vacuum (AQV) generation with metasurfaces. The solid green curve shows AQV, while the red dashed line shows boundaryless isotropic quantum vacuum. The inset shows a three-level atom in AQV, located at a certain macroscopic distance d from the metasurface plane, with two coupled orthogonal transitions among different states (from b to a_1 and from b to a_2 , respectively). The coherence between the transitions is defined as κ . (b) Phase profile of the designed metasurface. The phase shift is different for two orthogonal linear polarizations. (c) 2D presentation of the metasurface phase profile (denoted by the pseudocolor map). The inset shows a small region of the metasurface. (d) Schematic view of a multi-quantum-well (MQW) substrate with a plasmonic metasurface. The gold nanoantennas are placed on top of a MQW substrate, with a layer of platinum and another layer of gold below the substrate. The whole structure is placed in an indium phosphide (InP) layer. The design of the nanoantenna is also shown (unit: nm). Through intersubband transitions and gold nanoantennas, second-order optical nonlinearity can be significantly enhanced. (e) Conceptual image of second harmonic generation. It shows the generation of the frequency-doubled light (frequency 2ω) from incident light (frequency ω) with the MQW and the metasurface. (f) Change in second-harmonic-generation power conversion efficiency with the power (or intensity) of a fundamental frequency (FF) beam with the yyy polarization combination. The yyy polarization combination indicates the process in which the y -polarized second harmonic wave is generated by two y -polarized incident light. Adapted from Reference 81 (panels a–c) and Reference 83 (panels d–f), with permission.

effects with metasurfaces. Nonlinear metasurfaces, as the name implies, combine the advantages of metasurface-based flat optics and nonlinear optics, providing a new perspective for researchers to improve the performance and develop new functionalities of metasurfaces.

9.1. Nonlinearity Enhancement

One of the most critical tasks in nonlinear optics research is to generate large optical nonlinearity. In traditional nonlinear optics, optical nonlinearity can be generated from nonlinear optical materials, such as optical crystals and plasmonic materials (82), or it can be generated from external modulations through physical effects, such as the Pockels effect of birefringence. Normally, optical nonlinearities are very small. A recent study suggested a new way to achieve giant nonlinearity

with metasurface structures by using quantum-engineered electronic intersubband transitions in n -doped multi-quantum-well (MQW) heterostructures (83). A nonlinear optical response was generated from external optical pumping on a layered MQW substrate, and the nonlinear response was significantly enhanced by a metasurface consisting of arrays of plasmonic nanoantennas. Panels *d* and *e* of **Figure 6** show the design and schematic of the MQW-metasurface combination and the enhancement of the optical nonlinearity. The generation of nonlinearity could also be realized through external voltage bias, and such giant nonlinearity could facilitate wave mixing experiments, as well as photon pair generation in quantum communication.

9.2. Phase Control in Nonlinear Four-Wave Mixing

Another important application of the metasurface in nonlinear optics is that it can achieve the anomalous phase-matching condition of four-wave mixing (FWM) fields. With the phase gradient of the metasurface, an extra momentum/wave vector term is introduced in the phase-matching condition of the FWM wave, resulting in a new, anomalous phase-matching condition. Almeida et al. (84) thoroughly studied this phase-matching condition for FWM waves. Two transform-limited laser pulses interact with the nanocavities of the metasurface, generating FWM waves. Such FWM emissions can be steered by designing the phase gradient of the metasurface. The supercells of multiple nanocavities also form an optical blazed grating, which shows correspondence with the Raman-Nath diffraction theory in nonlinear optics. Almeida et al. (84) envisioned the nonlinear phase control of optical waves, and nonlinearity-based imaging devices might benefit from this study.

10. TUNABLE AND RECONFIGURABLE METASURFACES

Above, we discuss in detail the applications of the metasurface to various areas and its capability for light manipulation. Recently, there has been a rising demand in modern optical systems for switchable or tunable responses with changes in operational conditions. Such demand requires that the device be tuned or reconfigured. The metasurface, as a promising choice for realizing compact optical systems, suffers from a fixed response once it is fabricated. Therefore, researchers have put much effort into the realization of reconfigurable metasurfaces (85–89). Several feasible approaches were proposed and studied. In those approaches, functional materials, whose optical properties (e.g., permittivity) could be tuned from external stimuli, have been used as an additional degree of freedom to adjust the device. Some common types of such external stimuli are mechanical force, heat, optical field, magnetic field, and electric field. We briefly discuss here the tunable or reconfigurable metasurfaces based on the methods discussed in the subsections below.

10.1. Mechanically Tuned

One way to tune the response of metasurfaces with mechanical forces is by fabricating nanoantenna arrays on a flexible substrate, of which the most common is polydimethylsiloxane (PDMS). By stretching the substrate, the spacing between nanoantennas can be changed, similar to the case schematically shown in **Figure 7a**. Since metasurface functionality originates from the nanoantenna arrays, this change in relative position of the nanoantennas could result in a change in the metasurface's properties.

In a recent work (86), such a stretchable substrate was used to fabricate a metasurface with tunable phase gradient. An array of gold nanoantennas was placed on a PDMS substrate, with spatially varying orientation and shape to generate a phase gradient. The phase gradient changes

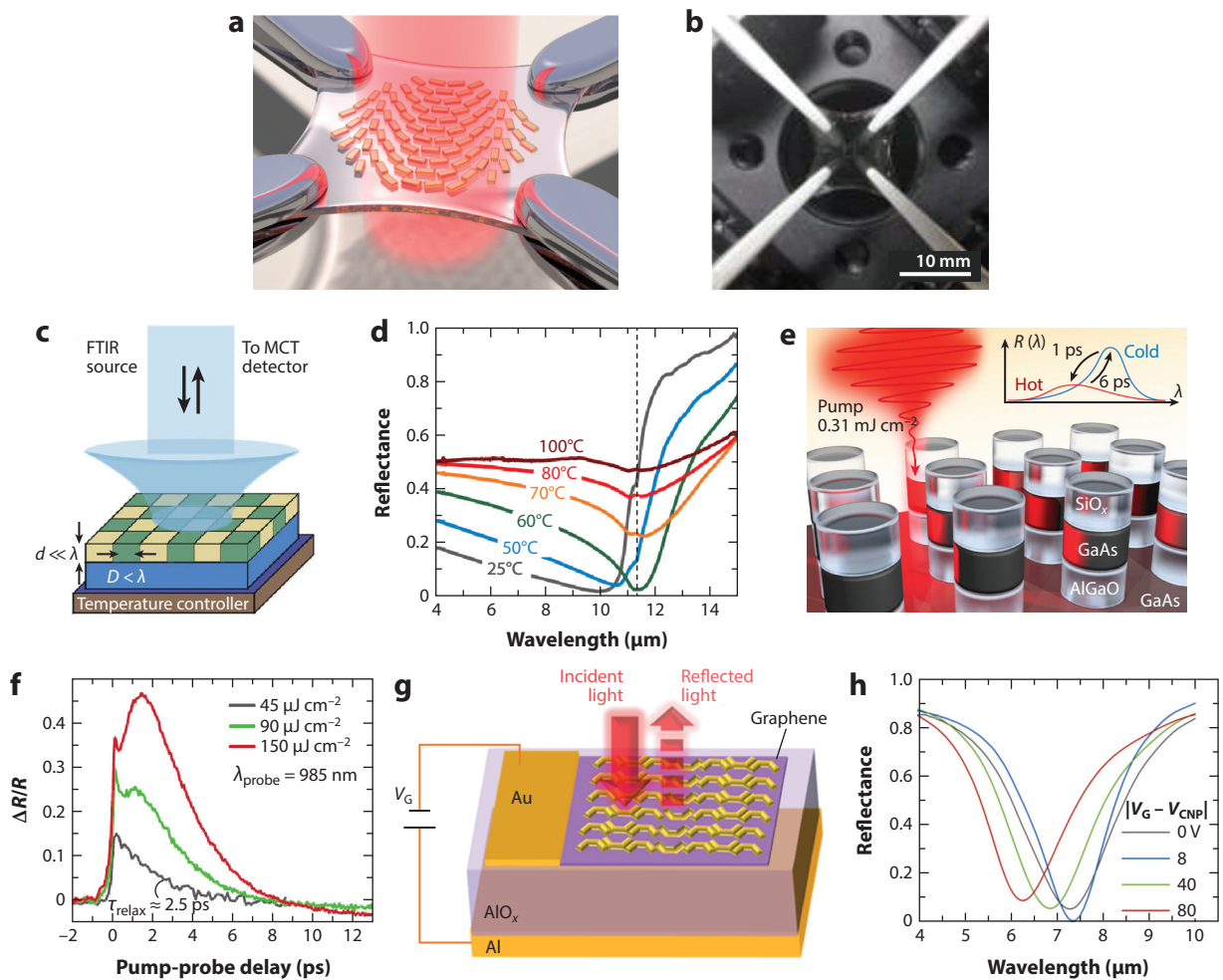


Figure 7

(a) Conceptual image of a stretched metasurface with a flexible substrate. The incident light (depicted in red) passes through a stretched metasurface with gold nanoantennas (depicted by yellow blocks). (b) A photo of flexible metalenses. The optical response of these metalenses could be tuned by mechanical stretching. (c) A schematic view of a temperature-tuned checkerboard metasurface. The blue layer represents a sapphire film with a thickness of D . The checkerboard structure is the vanadium dioxide region with a thickness of d , which results from selective defect engineering of the vanadium dioxide layer. Reflectance under near-normal incidence is measured using a Fourier transform infrared spectroscopy (FTIR) microscope. In this setup, an MCT (mercury cadmium telluride, or HgCdTe) detector is used to measure the intensity of the reflected light. (d) Experimental result of the measured reflectance. A strong dependency on temperature can be observed. As shown here, the reflectance reaches its minimum at 60°C at a wavelength $\lambda = 11.3 \mu\text{m}$, as denoted by the dashed vertical line. (e) Illustration of a GaAs metasurface being tuned by a femtosecond laser pulse. The inset shows the tuning and recovery of the magnetic dipole resonance. (f) Measured transient reflectance trace of the metasurface. $\Delta R = R_{\text{pump}} - R$, where R is reflectance in the absence of the pump beam and R_{pump} is reflectance in the presence of the pump beam. A strong correlation between the relative reflectance change, $\Delta R/R$, and the pumping power can be observed. (g) A schematic view of a metasurface absorber tuned by external voltage bias. (h) Measured reflectance under different voltage biases. V_G is the externally applied gate voltage, and V_{CNP} is the gate voltage when the concentrations of electrons and holes in the graphene sheet are equal. A clear dependency on external voltage bias could be observed. Adapted from Reference 86 (panels a and b), Reference 88 (panels c and d), Reference 94 (panels e and f), and Reference 95 (panels g and h), with permission.

when the PDMS substrate is stretched, resulting in a tunable refraction angle from 11.4° to 14.9° . On the basis of this result, a flat zoom lens, as shown in **Figure 7b**, can be fabricated with reconfigurable focal length. Such stretchable metasurfaces are expected to be integrated into wearable electronic devices or flat display systems, for which elastic materials are preferred.

10.2. Thermally Tuned

Changes in external temperature could also vary the optical response of a metasurface. To achieve temperature-tunable metasurfaces, a special kind of material, phase change materials (PCMs), are usually used to obtain large changes in optical properties. One typical example of a PCM is vanadium dioxide (VO_2) (90–92), which is in the insulator state with low conductivity at lower temperature but shifts to the metallic state with orders-of-magnitude-higher conductivity when heated to higher temperature. This metal-insulator transition (MIT) (90) originates from the internal lattice change of VO_2 and occurs near room temperature (approximately 340 K), which makes VO_2 amenable to thermal modulation.

Designs of VO_2 -based metasurfaces have been proposed and realized, achieving dynamic switching of optical responses. For instance, in 2016 Rensberg et al. (88) presented a design of an active metasurface based on a defect-engineered PCM. This work utilized ion beam irradiation to engineer the MIT and to make it happen at a lower temperature. A metasurface-based absorber was fabricated and characterized. Temperature-dependent reflectance was observed, as shown in **Figure 7c**. The temperature-dependent reflection spectra (**Figure 7d**) indicate the existence of the MIT during the heating process. Such PCMs enable new possibilities for metasurface design, and the thermally tunable metasurface could find its application in various fields, such as optical sensing and tunable thermal emission.

10.3. Optically Tuned

Modulation through optical pumping is commonly realized in ultrafast optics. With modulation using ultrafast light pulses, optical modulation could achieve much faster modulation speed than could traditional electrical modulation devices (93). A recent research paper (94) demonstrated, for the first time, free carrier-induced absolute reflectance modulation under low pumping power and fast recovery time. The researchers utilized direct-gap Mie-resonant semiconductor materials such as GaAs to generate free carriers under external optical pumping, and the position of magnetic dipolar resonance was shifted under such modulation, as shown in **Figure 7e**. In addition, the researchers also measured the time window of such free carrier injection and the recombination time. The result indicates that GaAs-based metasurfaces could achieve a much shorter relaxation time (approximately 2 ps) under lower pumping power than could silicon (approximately 30 ps). Moreover, optical pumping also changes the reflection spectra of the metasurface (**Figure 7f**). The researchers state that this phenomenon is due to the direct-gap nature of GaAs nanostructures. Such metasurfaces could work at visible frequencies as well as in the near-infrared regime with the appropriate semiconductor materials.

10.4. Electrically Tuned

Electrical tuning of material properties has been widely used with materials like graphene, which is a material with high electrical conductivity, broadband electro-optical properties, and stable chemical resistance (95, 96). By applying external voltage to a graphene layer, the carrier density of graphene can be adjusted, and thus its optical properties can be changed. A novel design of an

electrically tunable metasurface-based perfect absorber was presented on the basis of this principle (Figure 7g). Such an absorber has voltage-dependent reflectance (as measured in Figure 7b) and could be used in an optical modulator with a maximum modulation depth of more than 95% and a modulation speed of up to the tens of gigahertz in the mid-infrared range.

Many electro-optical materials other than graphene have been used in electrically tuned metasurface systems such as indium tin oxide (ITO). The permittivity of ITO can be tuned with external voltage, and such changes in permittivity will result in a change in the reflection spectra since the epsilon-near-zero (ENZ) frequency of the ITO is shifted. A recent study (87) utilized this property of ITO and integrated ITO into a silicon grating metasurface on a silica substrate. In this work, a positive external voltage bias was used to shift the ENZ frequency of ITO to 1.48 μm . The reflection near 1.48 μm changed from more than 95% to near zero.

11. TOPOLOGICAL METASURFACES

A common first impression of the word topology usually comes from the famous example of the topological equality between a doughnut and a teacup, which can be continuously deformed into each other. Rooted in abstract mathematics, topology was surprisingly utilized in research of condensed matter physics in the past 10 years, leading to the Nobel Prize-winning theory of topological insulators (97–99). Today, researchers are striving to extend the concept of topology to the optical regime, opening a new avenue of topological photonics.

In general, several methods are commonly used to introduce topological phases into a photonic system (100): breaking time-reversal symmetry, conservation of discrete degrees of freedom such as spin and valley, and spatial/temporal modulation. Experimental realizations of photonic topological insulators based on these methods have been reported to exploit photonic crystals. Metasurfaces, reported in a recent manuscript (101), could also be designed to exhibit band inversion by certain symmetry reduction. In this reported work, the optical scattering property of the metasurface could be controlled by tuning the synthetic gauge field, and the topological invariant (spin Chern number) of such a metasurface could be extracted through the measurement of transmission spectra.

The research on topological photonic systems has provided us with the possibility for previously unforeseen optical devices, such as robust delay lines, nonreciprocal devices, arbitrary geometry lasing (102), and much more. The metasurface, as an artificially designed structure, could be modified to introduce symmetry reduction and could be modulated spatially and temporally with optical pumping, external voltages, and other stimuli, providing numerous methods to form synthetic gauge fields for band inversion and topological phase transition. Therefore, we can expect that the combination of metasurfaces and topological photonics will further broaden our horizons and that the unique properties of such a combination are bound to be useful in future photonic systems.

12. CONCLUSION AND OUTLOOK

In this review article, we discuss in detail metasurfaces, from concept and theories to applications. The exotic optical properties of metasurfaces originate from the distributions of meta-atoms. The subwavelength spacing of those meta-atoms enables the manipulation of light with high spatial resolution. By engineering such meta-atoms, metasurfaces can have total control over various properties of light, such as phase, polarization, and amplitude. The metasurface technique provides a novel approach to create optical components and devices in an ultrathin layer and has led to applications in many fields. In addition, the fabrication of metasurfaces can be compatible with

the current lithography techniques in the semiconductor industry. Therefore, metasurfaces have great potential in building compact on-chip optical devices. In addition, by using novel materials with variable optical properties, reconfigurable and tunable metasurfaces can be realized.

Research on metasurfaces is rapidly growing. We conclude this review by envisioning some of the most important research areas of metasurfaces, with the hope of providing strategic guidance for fellow researchers.

1. One future research area is discovering and synthesizing materials with novel properties as constituents for metasurfaces. In the past decade, the emergence of novel materials such as graphene, ITO, VO₂, and titanium nitride has inspired wide applications. These materials, with their unique properties, manifest new functionalities of metasurfaces. In particular, low-loss plasmonic materials for metasurfaces are in great demand, as such materials can overcome the high loss of traditional plasmonic materials without losing the nice features of plasmonic resonances.
2. Another area to explore is metasurfaces with broadband response and reconfigurability. Many functions of traditional optical devices have been realized with metasurfaces. However, the great limitations of metasurfaces are their low bandwidth and high spectral dispersion. High bandwidth and low spectral dispersion are critical for many optical elements such as lenses. Moreover, to create devices such as displays and spatial light modulators, metasurfaces should be able to change their properties dynamically. There is great demand for the design and realization of a fully reconfigurable metasurface.
3. A third area for discovery is the integration of metasurfaces into current existing systems. In this review, we discuss the use of metasurfaces in immersion objective lenses and optical nonlinearity enhancement. Integrating metasurfaces with existing systems could be the shortest way to push the metasurface technology into industry. This idea could be applied to a vast variety of fields, including biomedical sensing and imaging, optical communication, lasers, and thermal detectors.

DISCLOSURE STATEMENT

The authors are not aware of any affiliations, memberships, funding, or financial holdings that might be perceived as affecting the objectivity of this review.

ACKNOWLEDGMENTS

We acknowledge support from the Gordon and Betty Moore Foundation and the Penn State MRSEC, the Center for Nanoscale Science, under award number NSF DMR-1420620.

LITERATURE CITED

1. Cai W, Shalaev V. 2010. *Optical Metamaterials*. New York, NY: Springer
2. Kildishev AV, Boltasseva A, Shalaev VM. 2013. Planar photonics with metasurfaces. *Science* 339(6125):1232009
3. Yu N, Capasso F. 2014. Flat optics with designer metasurfaces. *Nat. Mater.* 13(2):139–50
4. Mittra R, Chan CH, Cwik T. 1988. Techniques for analyzing frequency selective surfaces—a review. *Proc. IEEE* 76(12):1593–615
5. Meinzer N, Barnes WL, Hooper IR. 2014. Plasmonic meta-atoms and metasurfaces. *Nat. Photon.* 8(12):889–98
6. Mühlischlegel P, Eisler H-J, Martin OJF, Hecht B, Pohl DW. 2005. Resonant optical antennas. *Science* 308(5728):1607–9



7. Maier SA, Atwater HA. 2005. Plasmonics: localization and guiding of electromagnetic energy in metal/dielectric structures. *J. Appl. Phys.* 98(1):011101
8. Luk'yanchuk B, Zheludev NI, Maier SA, Halas NJ, Nordlander P, et al. 2010. The Fano resonance in plasmonic nanostructures and metamaterials. *Nat. Mater.* 9(9):707–15
9. Yu N, Genevet P, Kats MA, Aieta F, Tetienne J-P, et al. 2011. Light propagation with phase discontinuities: generalized laws of reflection and refraction. *Science* 334(6054):333–37
10. Ni X, Emani NK, Kildishev AV, Boltasseva A, Shalaev VM. 2011. Broadband light bending with plasmonic nanoantennas. *Science* 335:427
11. Sun S, He Q, Xiao S, Xu Q, Li X, Zhou L. 2012. Gradient-index meta-surfaces as a bridge linking propagating waves and surface waves. *Nat. Mater.* 11(5):426–31
12. Sun S, Yang K-Y, Wang C-M, Juan T-K, Chen WT, et al. 2012. High-efficiency broadband anomalous reflection by gradient meta-surfaces. *Nano Lett.* 12(12):6223–29
13. Berry MV. 1987. The adiabatic phase and Pancharatnam's phase for polarized light. *J. Mod. Opt.* 34(11):1401–7
14. Pancharatnam S. 1956. Generalized theory of interference, and its applications. *Proc. Indian Acad. Sci. A* 44(5):247–62
15. Boltasseva A, Atwater HA. 2011. Low-loss plasmonic metamaterials. *Science* 331(6015):290–91
16. Jahani S, Jacob Z. 2016. All-dielectric metamaterials. *Nat. Nanotechnol.* 11(1):23–36
17. Kuznetsov AI, Miroshnichenko AE, Brongersma ML, Kivshar YS, Luk'yanchuk B. 2016. Optically resonant dielectric nanostructures. *Science* 354(6314):aag2472
18. Mie G. 1908. Beiträge zur Optik trüber Medien, speziell kolloidaler Metallösungen. *Ann. Phys.* 330(3):377–445
19. Ginn JC, Brener I, Peters DW, Wendt JR, Stevens JO, et al. 2012. Realizing optical magnetism from dielectric metamaterials. *Phys. Rev. Lett.* 108(9):097402
20. Fu YH, Kuznetsov AI, Miroshnichenko AE, Yu YF, Luk'yanchuk B. 2013. Directional visible light scattering by silicon nanoparticles. *Nat. Commun.* 4:1527
21. Decker M, Staude I, Falkner M, Dominguez J, Neshev DN, et al. 2015. High-efficiency dielectric Huygens' surfaces. *Adv. Opt. Mater.* 3(6):813–20
22. Kerker M, Wang D-S, Giles CL. 1983. Electromagnetic scattering by magnetic spheres. *J. Opt. Soc. Am.* 73(6):765–67
23. Limonov MF, Rybin MV, Poddubny AN, Kivshar YS. 2017. Fano resonances in photonics. *Nat. Photon.* 11(9):543–54
24. Fedotov VA, Rose M, Prosvirnin SL, Papasimakis N, Zheludev NI. 2007. Sharp trapped-mode resonances in planar metamaterials with a broken structural symmetry. *Phys. Rev. Lett.* 99(14):147401
25. Miroshnichenko AE, Kivshar YS. 2012. Fano resonances in all-dielectric oligomers. *Nano Lett.* 12(12):6459–63
26. Fan P, Yu Z, Fan S, Brongersma ML. 2014. Optical Fano resonance of an individual semiconductor nanostructure. *Nat. Mater.* 13(5):471–75
27. Yan J, Liu P, Lin Z, Wang H, Chen H, et al. 2015. Directional Fano resonance in a silicon nanosphere dimer. *ACS Nano* 9(3):2968–80
28. King NS, Liu L, Yang X, Cerjan B, Everitt HO, et al. 2015. Fano resonant aluminum nanoclusters for plasmonic colorimetric sensing. *ACS Nano* 9(11):10628–36
29. Stern L, Grajower M, Levy U. 2014. Fano resonances and all-optical switching in a resonantly coupled plasmonic-atomic system. *Nat. Commun.* 5:4865
30. Yang Y, Wang W, Boulesbaa A, Kravchenko II, Briggs DP, et al. 2015. Nonlinear Fano-resonant dielectric metasurfaces. *Nano Lett.* 15(11):7388–93
31. Bomzon Z, Kleiner V, Hasman E. 2001. Pancharatnam-Berry phase in space-variant polarization-state manipulations with subwavelength gratings. *Opt. Lett.* 26(18):1424–26
32. Biener G, Niv A, Kleiner V, Hasman E. 2002. Formation of helical beams by use of Pancharatnam-Berry phase optical elements. *Opt. Lett.* 27(21):1875–77
33. Bomzon Z, Biener G, Kleiner V, Hasman E. 2002. Space-variant Pancharatnam-Berry phase optical elements with computer-generated subwavelength gratings. *Opt. Lett.* 27(13):1141–43



34. Feynman RP, Leighton RB, Sands M. 2011. *The Feynman Lectures on Physics, Vol. II: The New Millennium Edition: Mainly Electromagnetism and Matter*. New York: Basic Books. 594 pp.
35. Hirsch JE. 1999. Spin hall effect. *Phys. Rev. Lett.* 83(9):1834–37
36. Onoda M, Murakami S, Nagaosa N. 2004. Hall effect of light. *Phys. Rev. Lett.* 93(8):083901
37. Leyder C, Romanelli M, Karr JP, Giacobino E, Liew TCH, et al. 2007. Observation of the optical spin Hall effect. *Nat. Phys.* 3(9):nphys676
38. Hosten O, Kwiat P. 2008. Observation of the spin Hall effect of light via weak measurements. *Science* 319(5864):787–90
39. Bliokh KY, Bliokh YP. 2006. Conservation of angular momentum, transverse shift, and spin Hall effect in reflection and refraction of an electromagnetic wave packet. *Phys. Rev. Lett.* 96(7):073903
40. Liu Y, Ling X, Yi X, Zhou X, Chen S, et al. 2015. Photonic spin Hall effect in dielectric metasurfaces with rotational symmetry breaking. *Opt. Lett.* 40(5):756–59
41. Yin X, Ye Z, Rho J, Wang Y, Zhang X. 2013. Photonic spin Hall effect at metasurfaces. *Science* 339(6126):1405–7
42. Ni X, Ishii S, Kildishev AV, Shalaev VM. 2013. Ultra-thin, planar, Babinet-inverted plasmonic metalenses. *Light Sci. Appl.* 2(4):e72
43. Aieta F, Genevet P, Kats M, Capasso F. 2013. Aberrations of flat lenses and aplanatic metasurfaces. *Opt. Express* 21(25):31530–39
44. Aieta F, Kats MA, Genevet P, Capasso F. 2015. Multiwavelength achromatic metasurfaces by dispersive phase compensation. *Science* 347(6228):1342–45
45. Khorasaninejad M, Shi Z, Zhu AY, Chen WT, Sanjeev V, et al. 2017. Achromatic metalens over 60 nm bandwidth in the visible and metalens with reverse chromatic dispersion. *Nano Lett.* 17(3):1819–24
46. Khorasaninejad M, Zhu AY, Roques-Carmes C, Chen WT, Oh J, et al. 2016. Polarization-insensitive metalenses at visible wavelengths. *Nano Lett.* 16(11):7229–34
47. Zhang S, Kim M-H, Aieta F, She A, Mansuripur T, et al. 2016. High efficiency near diffraction-limited mid-infrared flat lenses based on metasurface reflectarrays. *Opt. Express* 24(16):18024
48. Byrnes SJ, Lenef A, Aieta F, Capasso F. 2016. Designing large, high-efficiency, high-numerical-aperture, transmissive meta-lenses for visible light. *Opt. Express* 24(5):5110
49. Khorasaninejad M, Chen WT, Oh J, Capasso F. 2016. Super-dispersive off-axis meta-lenses for compact high resolution spectroscopy. *Nano Lett.* 16(6):3732–37
50. Shaltout A, Liu J, Kildishev A, Shalaev V. 2015. Photonic spin Hall effect in gap-plasmon metasurfaces for on-chip chiroptical spectroscopy. *Optica* 2(10):860–63
51. Chen WT, Zhu AY, Khorasaninejad M, Shi Z, Sanjeev V, Capasso F. 2017. Immersion meta-lenses at visible wavelengths for nanoscale imaging. *Nano Lett.* 17(5):3188–94
52. Groever B, Chen WT, Capasso F. 2017. Meta-lens doublet in the visible region. *Nano Lett.* 17(8):4902–7
53. Hecht E. 2013. *Optics*. Boston: Pearson. 680 pp.
54. Balthasar Mueller JP, Rubin NA, Devlin RC, Groever B, Capasso F. 2017. Metasurface polarization optics: independent phase control of arbitrary orthogonal states of polarization. *Phys. Rev. Lett.* 118(11):113901
55. Yu N, Aieta F, Genevet P, Kats MA, Gaburro Z, Capasso F. 2012. A broadband, background-free quarter-wave plate based on plasmonic metasurfaces. *Nano Lett.* 12(12):6328–33
56. Arbabi A, Horie Y, Bagheri M, Faraon A. 2015. Dielectric metasurfaces for complete control of phase and polarization with subwavelength spatial resolution and high transmission. *Nat. Nanotechnol.* 10(11):937
57. Yang Y, Wang W, Moitra P, Kravchenko II, Briggs DP, Valentine J. 2014. Dielectric meta-reflectarray for broadband linear polarization conversion and optical vortex generation. *Nano Lett.* 14(3):1394–99
58. Lin D, Fan P, Hasman E, Brongersma ML. 2014. Dielectric gradient metasurface optical elements. *Science* 345(6194):298–302
59. Willner AE, Wang J, Huang H. 2012. A different angle on light communications. *Science* 337(6095):655–56
60. Beijersbergen MW, Allen L, van der Veen HELO, Woerdman JP. 1993. Astigmatic laser mode converters and transfer of orbital angular momentum. *Opt. Commun.* 96(1):123–32
61. Wang J, Yang J-Y, Fazal IM, Ahmed N, Yan Y, et al. 2012. Terabit free-space data transmission employing orbital angular momentum multiplexing. *Nat. Photon.* 6(7):nphoton.2012.138



62. Gibson G, Courtial J, Padgett MJ, Vasnetsov M, Pas'ko V, et al. 2004. Free-space information transfer using light beams carrying orbital angular momentum. *Opt. Express* 12(22):5448–56
63. Beijersbergen MW, Coerwinkel RPC, Kristensen M, Woerdman JP. 1994. Helical-wave front laser beams produced with a spiral phaseplate. *Opt. Commun.* 112(5):321–27
64. Devlin RC, Ambrosio A, Rubin NA, Mueller JPB, Capasso F. 2017. Arbitrary spin-to-orbital angular momentum conversion of light. *Science*; <https://doi.org/10.1126/science.aao5392>
65. Karimi E, Schulz SA, De Leon I, Qassim H, Upham J, Boyd RW. 2014. Generating optical orbital angular momentum at visible wavelengths using a plasmonic metasurface. *Light Sci. Appl.* 3(5):e167
66. Li J, Pendry JB. 2008. Hiding under the carpet: a new strategy for cloaking. *Phys. Rev. Lett.* 101(20):203901
67. Ni X, Wong ZJ, Mrejen M, Wang Y, Zhang X. 2015. An ultrathin invisibility skin cloak for visible light. *Science* 349(6254):1310–14
68. Estakhri NM, Alù A. 2014. Ultra-thin unidirectional carpet cloak and wave front reconstruction with graded metasurfaces. *IEEE Antennas Wirel. Propag. Lett.* 13:1775–78
69. Hsu LY, Lepetit T, Kante B. 2015. Extremely thin dielectric metasurface for carpet cloaking. *Prog. Electromagn. Res.* 152:33–40
70. Dammann H, Görtler K. 1971. High-efficiency in-line multiple imaging by means of multiple phase holograms. *Opt. Commun.* 3(5):312–15
71. Genevet P, Capasso F. 2015. Holographic optical metasurfaces: a review of current progress. *Rep. Prog. Phys.* 78(2):024401
72. Zheng G, Mühlenbernd H, Kenney M, Li G, Zentgraf T, Zhang S. 2015. Metasurface holograms reaching 80% efficiency. *Nat. Nanotechnol.* 10(4):nnano.2015.2
73. Ni X, Kildishev AV, Shalaev VM. 2013. Metasurface holograms for visible light. *Nat. Commun.* 4:2807
74. Li Z, Kim M-H, Wang C, Han Z, Shrestha S, et al. 2017. Controlling propagation and coupling of waveguide modes using phase-gradient metasurfaces. *Nat. Nanotechnol.* 12(7):675–83
75. Lin J, Mueller JPB, Wang Q, Yuan G, Antoniou N, et al. 2013. Polarization-controlled tunable directional coupling of surface plasmon polaritons. *Science* 340(6130):331–34
76. Pors A, Nielsen MG, Bernardin T, Weeber J-C, Bozhevolnyi SI. 2014. Efficient unidirectional polarization-controlled excitation of surface plasmon polaritons. *Light Sci. Appl.* 3(8):e197
77. Sun W, He Q, Sun S, Zhou L. 2016. High-efficiency surface plasmon meta-couplers: concept and microwave-regime realizations. *Light Sci. Appl.* 5(1):e16003
78. Wintz D, Ambrosio A, Zhu AY, Genevet P, Capasso F. 2017. Anisotropic surface plasmon polariton generation using bimodal V-antenna based metastructures. *ACS Photon.* 4(1):22–27
79. Chang DE, Sørensen AS, Hemmer PR, Lukin MD. 2006. Quantum optics with surface plasmons. *Phys. Rev. Lett.* 97(5):053002
80. Chang DE, Thompson JD, Park H, Vuletić V, Zibrov AS, et al. 2009. Trapping and manipulation of isolated atoms using nanoscale plasmonic structures. *Phys. Rev. Lett.* 103(12):123004
81. Jha PK, Ni X, Wu C, Wang Y, Zhang X. 2015. Metasurface-enabled remote quantum interference. *Phys. Rev. Lett.* 115(2):025501
82. Li G, Zhang S, Zentgraf T. 2017. Nonlinear photonic metasurfaces. *Nat. Rev. Mater.* 2(5):17010
83. Lee J, Tymchenko M, Argyropoulos C, Chen P-Y, Lu F, et al. 2014. Giant nonlinear response from plasmonic metasurfaces coupled to intersubband transitions. *Nature* 511(7507):65–69
84. Almeida E, Shalem G, Prior Y. 2016. Subwavelength nonlinear phase control and anomalous phase matching in plasmonic metasurfaces. *Nat. Commun.* 7:10367
85. Wang Q, Rogers ETF, Gholipour B, Wang C-M, Yuan G, et al. 2015. Optically reconfigurable metasurfaces and photonic devices based on phase change materials. *Nat. Photon.* 10(1):nphoton.2015.247
86. Ee H-S, Agarwal R. 2016. Tunable metasurface and flat optical zoom lens on a stretchable substrate. *Nano Lett.* 16(4):2818–23
87. Kim SJ, Brongersma ML. 2017. Active flat optics using a guided mode resonance. *Opt. Lett.* 42(1):5–8
88. Rensberg J, Zhang S, Zhou Y, McLeod AS, Schwarz C, et al. 2016. Active optical metasurfaces based on defect-engineered phase-transition materials. *Nano Lett.* 16(2):1050–55
89. Di Falco A, Zhao Y, Alù A. 2011. Optical metasurfaces with robust angular response on flexible substrates. *Appl. Phys. Lett.* 99(16):163110



90. Aetukuri NB, Gray AX, Drouard M, Cossale M, Gao L, et al. 2013. Control of the metal-insulator transition in vanadium dioxide by modifying orbital occupancy. *Nat. Phys.* 9(10):661–66
91. Kats MA, Blanchard R, Zhang S, Genevet P, Ko C, et al. 2013. Vanadium dioxide as a natural disordered metamaterial: perfect thermal emission and large broadband negative differential thermal emittance. *Phys. Rev. X* 3(4):041004
92. Kaplan G, Aydin K, Scheuer J. 2015. Dynamically controlled plasmonic nano-antenna phased array utilizing vanadium dioxide. *Opt. Mater. Express* 5(11):2513–24
93. Lei DY, Appavoo K, Ligmajer F, Sonnefraud Y, Haglund RF, Maier SA. 2015. Optically-triggered nanoscale memory effect in a hybrid plasmonic-phase changing nanostructure. *ACS Photon.* 2(9):1306–13
94. Shcherbakov MR, Liu S, Zubyuk VV, Vaskin A, Vabishchevich PP, et al. 2017. Ultrafast all-optical tuning of direct-gap semiconductor metasurfaces. *Nat. Commun.* 8:17
95. Yao Y, Shankar R, Kats MA, Song Y, Kong J, et al. 2014. Electrically tunable metasurface perfect absorbers for ultrathin mid-infrared optical modulators. *Nano Lett.* 14(11):6526–32
96. Yao Y, Kats MA, Genevet P, Yu N, Song Y, et al. 2013. Broad electrical tuning of graphene-loaded plasmonic antennas. *Nano Lett.* 13(3):1257–64
97. Kosterlitz JM, Thouless DJ. 1972. Long range order and metastability in two dimensional solids and superfluids. (Application of dislocation theory). *J. Phys. C Solid State Phys.* 5(11):L124
98. Kosterlitz JM, Thouless DJ. 1973. Ordering, metastability and phase transitions in two-dimensional systems. *J. Phys. C Solid State Phys.* 6(7):1181
99. Hasan MZ, Kane CL. 2010. Topological insulators. *Rev. Mod. Phys.* 82(4):3045–67
100. Khanikaev AB, Shvets G. 2017. Two-dimensional topological photonics. *Nat. Photon.* 11(12):763–73
101. Gorlach MA, Ni X, Smirnova DA, Korobkin D, Slobzhanyuk AP, et al. 2017. Controlling scattering of light through topological transitions in all-dielectric metasurfaces. arXiv:1705.04236 [cond-mat.mtrl-sci]
102. Bahari B, Ndao A, Vallini F, Amili AE, Fainman Y, Kanté B. 2017. Nonreciprocal lasing in topological cavities of arbitrary geometries. *Science* 358(6363):636–40

